Neutron-powder-diffraction study of the magnetic and structural properties of $Pr_{0.6}(Ca_{1-x}Sr_x)_{0.4}MnO_3$ $(0 \leqslant x \leqslant 1)$

M. R. Lees, J. Barratt, G. Balakrishnan, and D. McK. Paul
Physics Department, University of Warwick, Coventry, CV4 7AL, United Kingdom

C. Ritter
Institut Laue Langevin, Boîte Postale 156, F-38042 Grenoble Cedex 9, France

(Received 6 November 1997)

We present the results of a neutron-powder-diffraction study in which we have examined the magnetic and structural properties of $Pr_{0.6}(Ca_{1-x}Sr_x)_{0.4}MnO_3$ $(0 \leqslant x \leqslant 1)$ as a function of doping concentration x and temperature. For $x \leqslant 0.15$ charge ordering and a Jahn-Teller distortion below 250 K are evident from rapid changes in the lattice parameters and bond lengths as a function of temperature and a transition from a high-temperature orthorhombic to a low-temperature monoclinic structure. For $x = 0.0$ the system orders antiferromagnetically at $T_N = 170$ K. At low temperature the system has a canted *CE* structure. As the temperature approaches T_N there is a transition to a collinear magnetic arrangement. For Sr doping of up to $x = 0.15$ the magnetic transition temperature remains almost constant but the magnetic arrangement now has a ferromagnetic component which persists up to T_N. For $x > 0.15$ the charge ordering is removed and the lattice parameters show a more normal temperature dependence. The materials are now simple ferromagnets and the ferromagnetic transition temperature T_C increases rapidly with x. [S0163-1829(98)02238-3]

I. INTRODUCTION

Perovskites of composition $R_{1-x}A_xMnO_3$ (R = rare earth and A = alkali earth) have attracted considerable interest because they display a range of extraordinary magnetic, electronic, and structural properties including colossal negative magnetoresistance,[1–3] charge ordering[4–9] and magnetic-field-induced changes in structure.[10,11] There have been many studies which have attempted to correlate the changes in structure with the variations in the nature of the magnetic ordering and the electronic properties of these systems. These have included studies as a function of doping across an entire series such as $La_{1-x}Ca_xMnO_3$ and $La_{1-x}Sr_xMnO_3$ (Refs. 12–14) and studies at fixed doping as a function of the dopant, particularly in the ferromagnetically ordered materials at $x = 0.3$.[1–3,15] Charge ordering (CO) has been reported in a number of materials near $x = 0.5$, for example, in $La_{0.5}Ca_{0.5}MnO_3$,[4–6] $Pr_{0.5}Sr_{0.5}MnO_3$,[7,8] and $Nd_{0.5}Sr_{0.5}MnO_3$.[9] CO has also been reported in systems such as $Pr_{1-x}Ca_xMnO_3$ which exhibits a thermally activated conductivity over the entire Ca concentration.[16–24] In this paper we describe the results of neutron-powder-diffraction study of materials with the composition $Pr_{0.6}(Ca_{1-x}Sr_x)_{0.4}MnO_3$ $(0 \leqslant x \leqslant 1)$. In this case, although the level of doping remains constant throughout the series, the two end compounds have been shown to exhibit very different properties. On the one hand, $Pr_{0.6}Ca_{0.4}MnO_3$ has a charge-ordering transition at 250 K and orders antiferromagnetically (AFM) with a *CE* magnetic structure below 170 K. In zero field it exhibits activated temperature dependence becoming an insulator below 50 K.[23] In contrast, $Pr_{0.6}Sr_{0.4}MnO_3$ is a ferromagnet (FM) with a Curie temperature T_C of 305 K.[7] The magnetic transition is accompanied by a switch from a resistivity with an activated temperature dependence, to a regime where the resistivity decreases with decreasing temperature (see Figs. 1 and 2). As a result this series of materials provides us with an excellent opportunity to study, at a constant level of alkali-earth doping, the sometimes competing, sometimes complementary phenomena displayed by this class of rare-earth manganites during the crossover from a material which is a charge ordered antiferromagnetic insulator to a ferromagnetic conductor.

II. EXPERIMENTAL DETAILS

Polycrystalline samples of $Pr_{0.6}(Ca_{1-x}Sr_x)_{0.4}MnO_3$ $(0 \leqslant x \leqslant 1)$ were prepared by a normal solid-state reaction

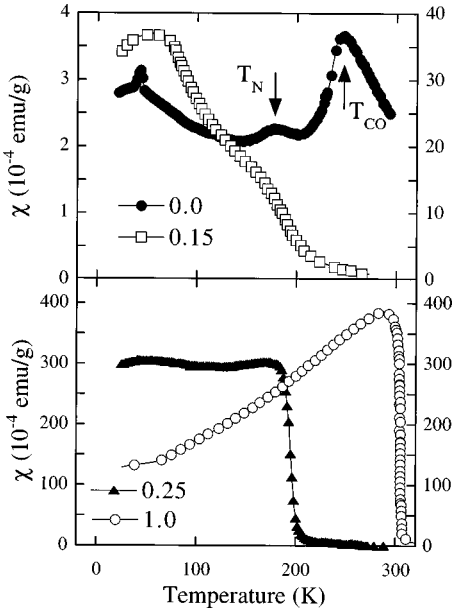

FIG. 1. Temperature dependence of the ac susceptibility for selected $Pr_{0.6}(Ca_{1-x}Sr_x)_{0.4}MnO_3$ samples. Open symbols refer to the right-hand scale, closed symbols to the left-hand scale.

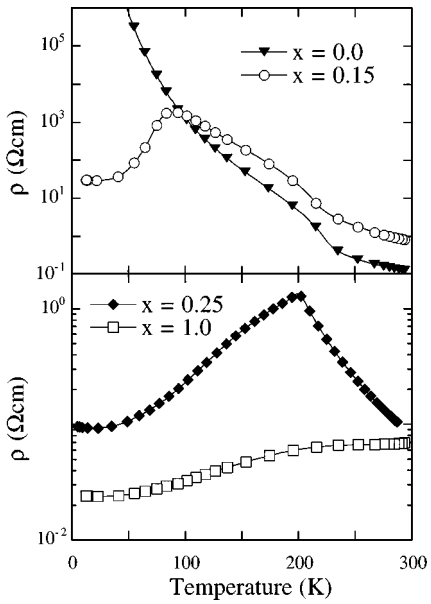

FIG. 2. Variation of resistivity with temperature for selected $Pr_{0.6}(Ca_{1-x}Sr_x)_{0.4}MnO_3$ samples.

route. Stoichiometric quantities of Pr_6O_{11}, $CaCO_3$, $SrCO_3$, and MnO_2 were repeatedly ground and then sintered in air for 12 h at a temperature of 1350 °C before finally being pressed and sintered at the same temperature for 24 h. X-ray analysis revealed all the samples to be single phase.

Neutron-powder-diffraction experiments were carried out at the Institut Laue-Langevin in order to study the crystallographic and magnetic structure of this series of compounds as a function of temperature and the Ca/Sr ratio. Diffraction patterns for seven samples ($x=0.0$, 0.12, 0.15, 0.25, 0.5, 0.75, and 1.0) were collected at different temperatures between 1.6 and 320 K using the D1B diffractometer. This high flux diffractometer operated at a wavelength of $\lambda = 2.52$ Å with a multidetector extending over 80° in 2Θ. After preliminary analysis of the data, the D2B diffractometer operating at a wavelength of $\lambda = 1.594$ Å over an angular range between 0° and 160° was used to collect higher resolution data required for detailed structural analysis. The nuclear and magnetic structures were refined by the Rietveld method using the program FULLPROF.[25]

III. EXPERIMENTAL RESULTS

A. Introduction

The observed properties of the $Pr_{0.6}(Ca_{1-x}Sr_x)_{0.4}MnO_3$ ($0 \leqslant x \leqslant 1$) system allow us to divide this series into three distinct composition regimes. Figure 3 shows the three-dimensional (3D) thermograms for samples with $x=0.0$, 0.10, and 0.25, which are typical of the materials in each of the three regions. The $x=0.00$ compound has a charge ordering transition at 250 K and orders antiferromagnetically with a CE magnetic structure below 170 K.[18,23] For low levels of Sr doping ($0.04 \leqslant x \leqslant 0.15$) the system is CO but now there is a coexistence of FM and AFM order. For $x \geqslant 0.2$ there is no evidence of a CO transition and the samples are simple ferromagnets. In the following we first describe in more detail the nature of the magnetic order across this series of compounds. We then discuss the evolution of the structural parameters as a function of temperature and doping level. Finally we briefly discuss our findings in the context of some of the simple models which have been used to understand the behavior of this class of materials.

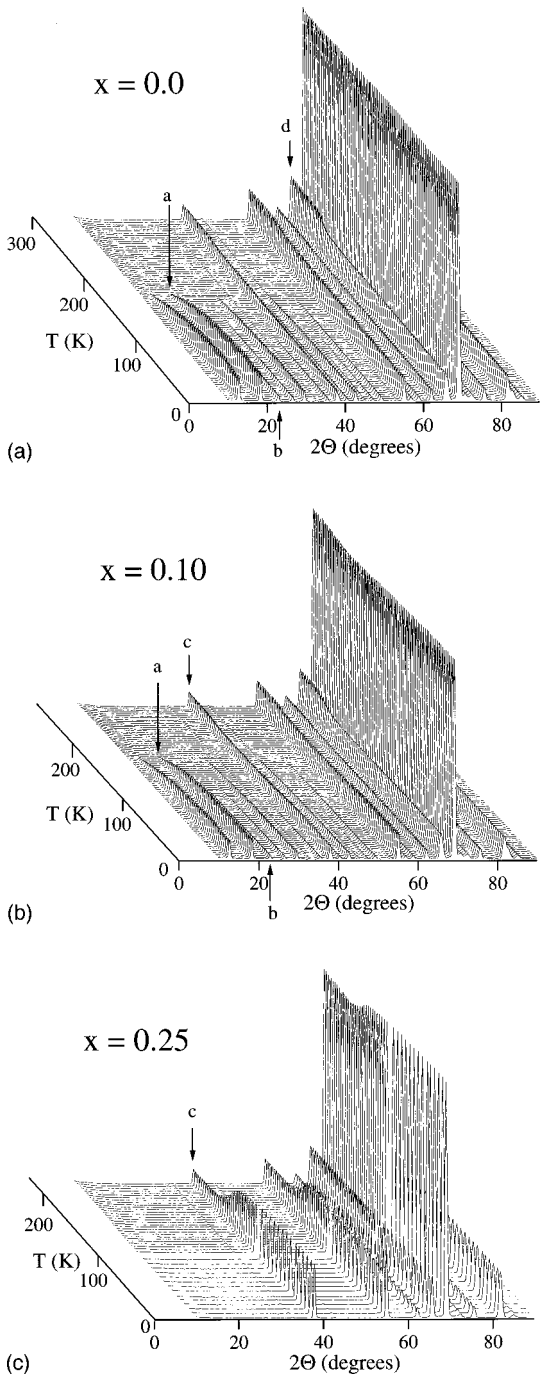

FIG. 3. 3D thermograms for samples of $Pr_{0.6}(Ca_{1-x}Sr_x)_{0.4}MnO_3$ with $x=0.0$, $x=0.10$, and $x=0.25$. The temperature dependence of the peaks labeled *a* (1/2, 1, 0), *b* (1/2, 0, 1), *c* (1, 1, 0), and *d* (1, 2, 1)/(2, 1, 1) are indicative of the temperature dependence of the antiferromagnetic ordering, the canted to collinear transition, ferromagnetic ordering, and the Jahn-Teller/charge-ordering transition, respectively.

B. Magnetic properties

For $x=0.0$ the system orders antiferromagnetically with a magnetic structure which changes considerably as a function of temperature. The magnetic lines in the diffraction pattern can be divided into two groups, one set with $h=$ half integer, $k=$ integer or half integer, $l=$ even and the other set with $h=$ half integer, $k=$ integer or half integer, $l=$ odd corresponding to moments along the [001] and [010] directions, respectively. At 1.5 K the system has a canted CE structure with colinear moments within each (001) plane and two distinct magnetic sublattices.[18] The magnitude of the moments are $M_y=1.52\mu_B$ and $M_z=2.29\mu_B$ giving $M=2.75\pm0.03\mu_B$ for the first (Mn^{3+}) sublattice and $M_y=1.19\mu_B$ and $M_z=2.44\mu_B$ giving $M=2.72\pm0.03\mu_B$ for the second (Mn^{4+}) sublattice. At 30 K there is a small increase in the value of the moments to $2.89\pm0.03\mu_B$ and $2.79\pm0.03\mu_B$. As the temperature increases the cant angle decreases and at $T_M=150$ K the y component on both the Mn^{3+} and Mn^{4+} sublattices is reduced to zero leaving magnetic moments of $1.39\pm0.03\mu_B$ and $1.51\pm0.03\mu_B$ respectively. This transition to a collinear structure is reflected in the difference in the temperature dependence of two sets of magnetic lines with odd and even l indices (see Fig. 4). The two sublattices are coupled together with a common T_N of 170 K. The substitution of a small amount of Sr results in a system which still has an antiferromagnetic CE structure. For example, in $Pr_{0.6}Ca_{0.34}Sr_{0.06}MnO_3$ the transition temperatures are now $T_M=150$ K and $T_N=180$ K. However, there is now also a ferromagnetic component to the magnetic order with the magnetic contributions to the peaks appearing on lines with h, $k=$ integer and $h+k=$ even. A plot of the observed versus calculated neutron-diffraction pattern for $Pr_{0.6}Ca_{0.34}Sr_{0.06}MnO_3$ is shown in Fig. 5(a). In this $x=0.15$ sample at 1.5 K, $M_x=1.63\mu_B$, $M_y=1.19\mu_B$, and $M_z=2.21\mu_B$ giving $M=2.99\pm0.03\mu_B$ for the first (Mn^{3+}) sublattice and $M_x=1.63\mu_B$, $M_y=1.01\mu_B$, and $M_z=2.26\mu_B$ giving $M=2.97\pm0.03\mu_B$ for the second (Mn^{4+}) sublattice. Again there is a small increase in the magnitude of the net moment at 30 K. In all the materials where AFM and FM coexist, the ferromagnetic component persists up to T_N. The temperature dependence of integrated intensities in the magnetic peaks which correspond to FM order also have an unusual temperature dependence (see Fig. 4) which makes the exact determination of T_C difficult. This type of behavior has previously been observed by Yoshizawa *et al.*[26] for a sample of $Pr_{0.65}(Ca_{1-x}Sr_x)_{0.35}MnO_3$ with $x=0.3$. We attribute this behavior to a coupling of the AFM and FM structures within these materials. As the concentration of x is increased further the system becomes purely ferromagnetic. $Pr_{0.6}Ca_{0.3}Sr_{0.1}MnO_3$ has a T_C of 175 K with magnetic moment below T_C of $3.3\mu_B$. For $x=0.5$, $x=0.75$, and $x=1.0$ compounds are also ferromagnetic. T_C increases with x (see Table I) with a magnetic moment of $\sim3.4\mu_B$ for all the compounds within this range of x. In this regime the temperature dependence of the magnetization appears to have a more normal behavior.

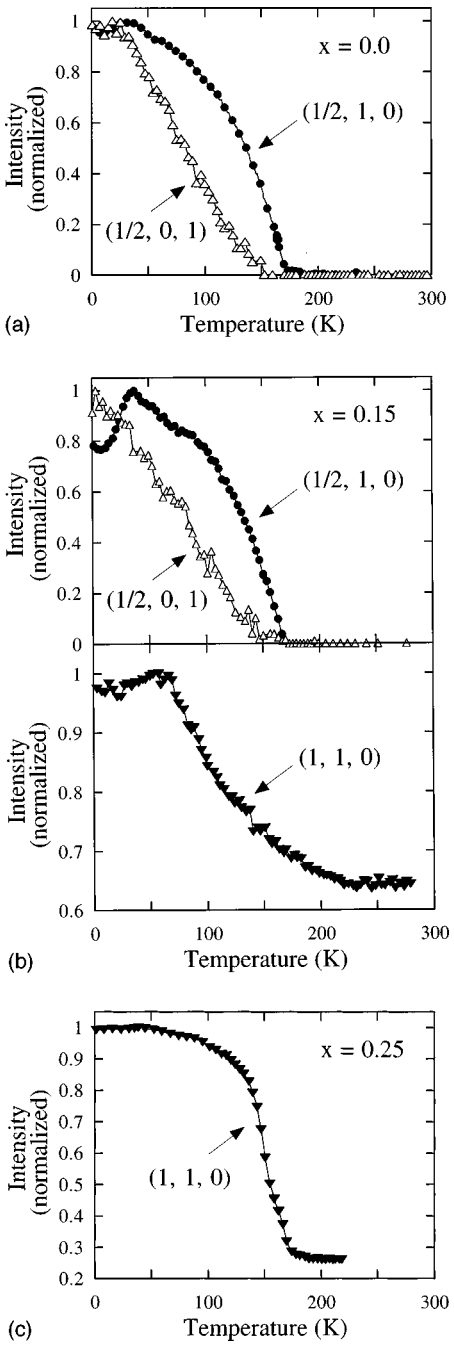

FIG. 4. Temperature dependence of selected lines in the neutron-powder-diffraction patterns of the samples of $Pr_{0.6}(Ca_{1-x}Sr_x)_{0.4}MnO_3$ with $x=0.0$, $x=0.15$, and $x=0.25$. For $x=0.0$ the (1/2, 1, 0) line is indicative of the onset of antiferromagnetic order with a CE structure at $T_N=175$ K. The variation in intensity of the (1/2, 0, 1) line reflects the switch from a collinear to a canted CE structure at $T_M=150$ K. For $x=0.15$ the variations of intensity with temperature of the (1/2, 1, 0) and (1/2, 0, 1) lines again reflect the evolution of the antiferromagnetic order. The additional magnetic intensity in the (1,1,0) line indicates the onset of ferromagnetic order, which is coupled to the antiferromagnetic order. For $x=0.25$ the additional ferromagnetic intensity in the (1,1,0) line shows a more normal temperature dependence.

C. Structual parameters

First we discuss the overall crystallographic structure of the materials. At room temperature all the materials examined have an orthorhombic *Pbnm* structure. The onset of charge ordering and the appearance of well defined Mn^{3+} and Mn^{4+} crystallographic sites are expected to be accompanied by lattice distortions due to the size difference between

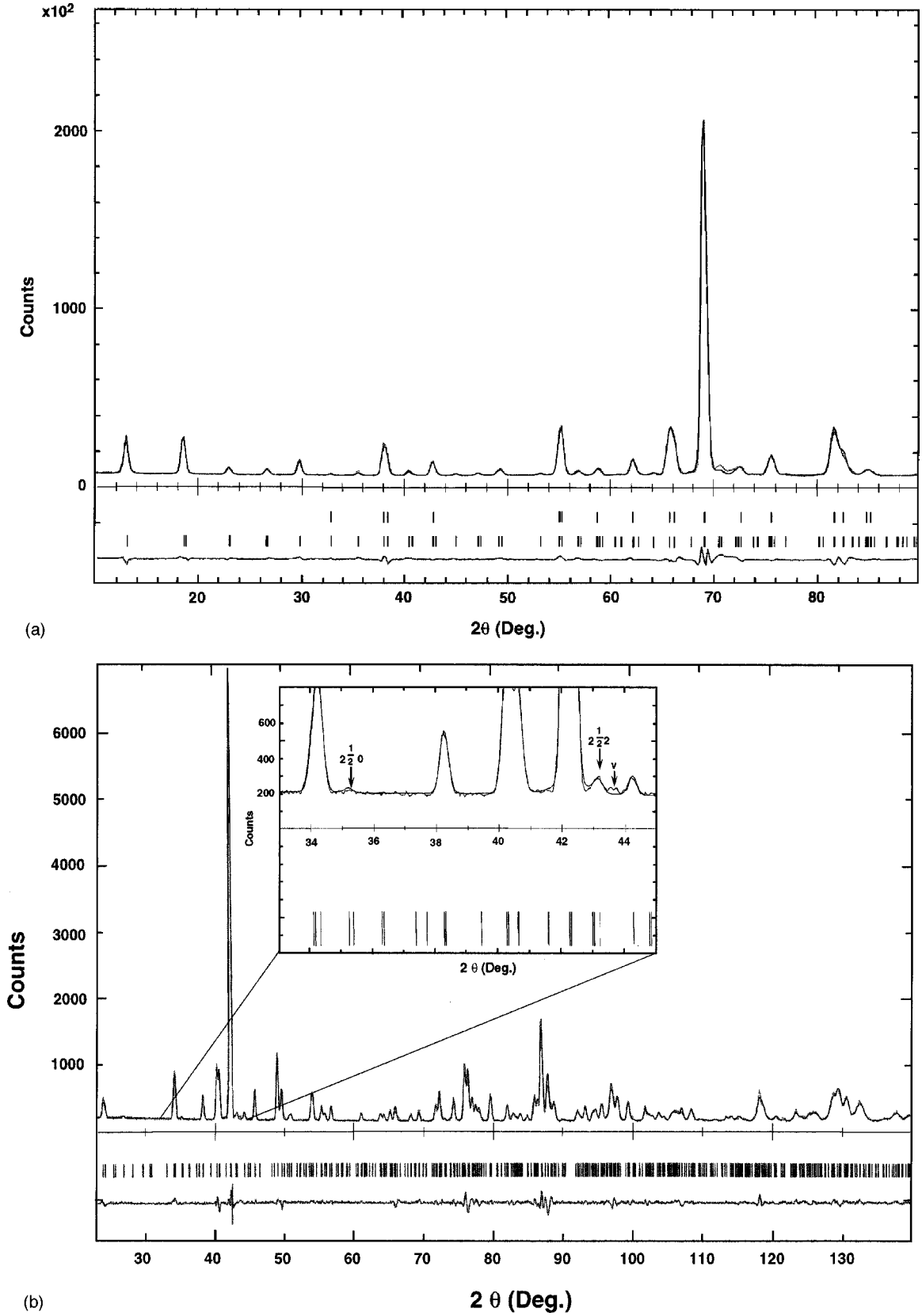

FIG. 5. (a) Powder-diffraction pattern for $Pr_{0.6}Ca_{0.34}Sr_{0.06}MnO_3$ ($x=0.15$) taken at $T=5$ K with $\lambda=2.52$ Å and a Rietveld refinement of the data. The difference between the observed and the calculated profiles is plotted at the bottom. (b) Powder-diffraction pattern for $Pr_{0.6}Ca_{0.4}MnO_3$ taken at $T=200$ K with $\lambda=1.594$ Å and a Rietveld refinement of the data. The difference between the observed and the calculated profiles is plotted at the bottom. The inset shows the superlattice peaks which appear below 250 K indicating the onset of charge ordering. The Miller indices refer to the high-temperature *Pbnm* setting. The peak labeled *v* comes from the vanadium sample can.

TABLE I. Selected magnetic parameters for samples of $Pr_{0.6}(Ca_{1-x}Sr_x)_{0.4}MnO_3$ ($0.0 \leqslant x \leqslant 1.0$).

x	T_M (K)	T_N (K)	M_{AFM1} (μ_B)	M_{AFM2} (μ_B)	T_C (K)	M (μ_B)
0.00	150	175	1.39±0.03 @ 150 K	1.51±0.03 @ 150 K		
			2.89±0.03 @ 30 K	2.79±0.03 @ 30 K		
			2.75±0.03 @ 1.5 K	2.72±0.03 @ 1.5 K		
0.10	130	170	2.95±0.03	2.9±0.03		
0.15	150	180	2.99±0.03	2.97±0.03		
0.25					175	3.3±0.03
0.50					250	3.4±0.03
0.75					275	3.45±0.03
1.00					305	3.3±0.03

the Mn^{3+} and Mn^{4+} ions. This could lead to the appearance of additional Bragg peaks which may either be associated with the difference in charge on the two Mn sites but are more likely to reflect the displacement of the Mn cations and the coordination oxygen atoms due to the different ionic radii and the Jahn-Teller distortions of the $Mn^{3+}O_6$ octahedra. In any event, such a CO distortion cannot be accommodated in the *Pbnm* space group and requires a reduction in the crystallographic symmetry. For $x=0.0$, a careful examination of spectra taken between 200 and 240 K, but above T_N, where the magnetic ordering greatly complicates the picture, reveals that the CO is indeed evident as a subtle distortion which produces changes in the widths of some lines and leads to the appearance of some superlattice peaks [see Fig. 5(b)]. The structure can then be indexed as $P2_1/m$. (Note *a*, *b*, and *c* in the $P2_1/m$ space group correspond to *b*, *c*, and *a*, respectively, in the *Pbnm* space group). The data has been fitted assuming a doubling of the unit cell along the *a* axis in the $P2_1/m$ setting. The four inequivalent sites in the *Pbnm* structure are increased to 15 for $P2_1/m$. The resulting increase in the number of atomic parameters requires that some are coupled during the refinement. The way in which the parameters have been coupled in this case can be deduced directly from the identical errors bars in the list of structural parameters given in Table II. The Mn^{3+} ions are left in the special positions 0, 0, 0 and $\frac{1}{2}$, 0, 0 while the Mn^{4+} at $\frac{1}{4}$, 0, $\frac{1}{2}$ and $\frac{3}{4}$, 0, $\frac{1}{2}$ are displaced along *c* in opposite directions to one another. The Pr(1) and Pr(3) ions shift in the same direction as the neighboring Mn^{4+} ion. The O1 oxygen atoms are left at the special positions *x*, $\frac{1}{4}$, *z*, while the O2 oxygen atoms are shifted to reduce the distortion around the Mn^{4+} site. As a result the Mn-O oxygen distances in the $Mn^{4+}O_6$ octahedra vary from 1.93 to 1.97 Å, while the Mn-O distances in the $Mn^{3+}O_6$ octahedra range from 1.89 to 2.02 Å [for Mn(2)] and 1.91 to 2.035 Å [for Mn(3)]. A similar monoclinic distortion has been observed for the $x=0.10$ sample. We note that Hervieu *et al.*[27] have recently published details of a high-resolution microscopy investigation of a sample of $Pr_{0.70}Ca_{0.25}Sr_{0.05}MnO_3$ in which they observed the presence of monoclinic domains within an orthorhombic *Pbnm* matrix, whilst Radaelli *et al.*[6] have proposed a similar monoclinic structure for $La_{0.5}Ca_{0.5}MnO_3$ in the CO state. In contrast, for samples with $x \geqslant 0.25$ there are no additional superstructure lines which appear below 250 K. We conclude that the CO transition does not take place in these Sr-rich samples. For $x \approx 1.0$ there is a low-temperature structural transition to a monoclinic $I2/a$ phase. A full discussion of this low-temperature phase transition has already been given in Ref. 28 and will not be repeated here.

We now consider the behavior of the internal structural parameters. For simplicity we have used the higher symmetry *Pbnm* space group in the refinements. This produces average values for bond lengths and bond angles. The structural information extracted in this way from the diffraction data including the variation with temperature and Ca/Sr doping ratio of the lattice parameters, Mn-O bond angles and Mn-O bond lengths are collected in Figs. 6–11 and Table III. For $x=0.0$ at room temperature, a double tilting of the MnO_6 octahedra produces an O orthorhombic structure with $b > a \geqslant c/\sqrt{2}$. Around 250 K we observe a rapid increase in the *a* and *b* lattice parameters, while *c* decreases producing an O′ orthorhombic structure with $b \geqslant a > c/\sqrt{2}$. Below 200 K the lattice parameters contract slowly as the temperature is reduced (see Fig. 6). Rapid changes in the Mn-O bond lengths are also observed around 250 K. There is an increase in the lengths of the equatorial Mn-O2 bonds and a decrease in the apical Mn-O1 distance. However, the net result is only a small decrease in the average Mn-O bond length. Below 200 K the values for the bond lengths are almost constant, so the average the Mn-O bond length ⟨Mn-O⟩ is virtually unchanged over the entire temperature range studied (see Figs. 7 and 8). The Mn-O-Mn bond angles also vary with temperature (see Fig. 9) although the magnitude of the variations are relatively small. The observed changes all mark an increase in the Jahn-Teller (JT) distortion and coincide with the onset of a CO transition which also occurs at $T \approx 250$ K. Similar behavior has been observed in samples with $x=0.10$ and $x=0.15$. It has been suggested that the distortions resulting from charge ordering and JT effects in this class of materials should be primarily metric in nature, i.e., associated with changes in the Mn-O bond lengths as opposed to distortions of the Mn-O bond angles.[29] For the Ca-rich samples studied here, in which these effects are most marked, this is certainly the case.

As expected, for the samples which have a simple FM ground state, i.e., for $0.25 \leqslant x \leqslant 1.0$, the structural parameters are well behaved at temperatures around 250 K. In fact, in this composition range, both the lattice parameters and the ⟨Mn-O⟩ bond lengths vary monotonically with temperature down to 1.5 K (see, e.g., the behavior for $x=0.5$ sample shown in Fig. 7). There have been several studies which have focused on the behavior of structural parameters of

TABLE II. Structural parameters for $Pr_{0.6}Ca_{0.4}MnO_3$ calculated using the orthorhombic P*bnm* and monoclinic $P2_1/m$ space groups at 200 K. A comparison between these two refinements indicates the distortions which arise as a result of the charge ordering transition. The refinement in the monoclinic $P2_1/m$ was made using several constraints. We began with the *Pbnm* atomic positions. The cell was doubled along the *a* direction in the $P2_1/m$ space group. Note *a*, *b*, and *c* in the $P2_1/m$ space group correspond to *b*, *c*, and *a*, respectively, in the *Pbnm* space group. The *z* parameter of the Mn(3) was varied. Then the *z* parameters for the Pr(1) and Pr(3) sites were allowed to follow the shift of the Mn(3). Finally the *z* parameters of the oxygen atoms in the Mn(3)-O_6 octahedra were refined. The apical O1(2) and O1(4) oxygen atoms are constrained to move in opposite directions while the equatorial oxygens O2(1)-O2(4) all move in the same direction. The numbers in parentheses are the statistical errors of the last significant digits.

Refined structural parameters in the *Pbnm* space group of $Pr_{0.6}Ca_{0.4}MnO_3$ at T=200 K

K

a(Å)	5.4310(2)		α(degrees)	90
b(Å)	5.4417(2)		β(degrees)	90
c(Å)	7.6022(3)		γ(degrees)	90
Atom	x	y	z	B
Pr	−0.0078(4)	0.0336(6)	0.25	0.59(4)
Mn	0.5	0.0	0.0	0.22(5)
O(1)	0.0704(5)	0.4878(5)	0.25	0.70(4)
O(2)	0.7168(4)	0.2842(4)	0.0369(2)	0.78(3)

Refined structural parameters in the $P2_1/m$ space group of $Pr_{0.6}Ca_{0.4}MnO_3$ at $T=200$ K

a(Å)	10.8826(4)		α(degrees)	90
b(Å)	7.6022(2)		β(degrees)	90
c(Å)	5.4313(2)		γ(degrees)	90
Atom	x	y	z	B
Pr(1)	0.2667(2)	0.25	−0.018(2)	0.62(4)
Pr(2)	3/4−Pr(1)	0.75	0.492(2)	0.62(4)
Pr(3)	1/2+Pr(1)	0.25	0.002(2)	0.62(4)
Pr(4)	1/2+Pr(2)	0.75	Pr(2)	0.62(4)
Mn(1)	0.0	0.0	0.0	0.21(5)
Mn(2)	0.5	0.0	0.0	0.21(5)
Mn(3)	0.25	0.0	0.485(3)	0.21(5)
O1(1)	0.4932(2)	0.25	0.0762(8)	0.66(4)
O1(2)	3/4−O1(1)	0.75	0.554(2)	0.66(4)
O1(3)	1/2+O1(1)	0.25	O1(1)(8)	0.66(4)
O1(4)	1/2+O1(2)	0.75	0.576(2)	0.66(4)
O2(1)	0.3922(2)	0.0373(2)	0.6985(6)	0.51(3)
O2(2)	3/4−O2(1)	1−O2(1)	O2(1)−1/2	0.51(3)
O2(3)	1/2+O2(1)	O2(1)	0.7330(5)	0.51(3)
O2(4)	1/2+O2(2)	1−O2(1)	O2(3)−1/2	0.51(3)

manganites around the ferromagnetic transition. Argyriou *et al.*[30] have reported on the temperature dependence of the structural parameters for an orthorhombic insulating sample of $La_{0.875}Sr_{0.125}MnO_3$ with a ferromagnetic ordering temperature T_C of 220 K. They showed that the *a* axis decreased smoothly with temperature while the *b* and *c* axis lattice parameters undergo pronounced changes with temperature. From room temperature down to 220 K the *c* axis exhibited a large positive thermal expansion, while the *b* axis had a large negative expansion. At T_C, the *c*-axis thermal expansion decreased, while the *b* axis thermal expansion increased. Below 100 K the unusual behavior disappeared. The internal structural parameters also show unusual temperature dependence. The apical Mn-O bond contracts slightly between 300 and 220 K before relaxing back to its room temperature value at 20 K. In contrast, the two equatorial Mn-O2 bond lengths change substantially (~0.05 Å) over a temperature interval centered around 220 K producing a large breathing motion in the plane of the MnO_6 octahedra. Although our data points are much more widely separated in temperature there is no evidence for similar breathing mode around T_C in any of our ferromagnetic samples. Radaelli *et al.*[29] have reported much smaller (~0.005 Å) anomalies in the Mn-O bond lengths around T_C in a sample of $La_{0.75}Ca_{0.25}MnO_3$, while Caignert *et al.*[31] have observed a decrease in the distortion of the MnO_6 octahedra at the transition to a ferromagnetically ordered state in a sample of $Pr_{0.7}(Ca_{1-x}Sr_x)_{0.3}MnO_3$ with $x=0.33$. In both cases the dif-

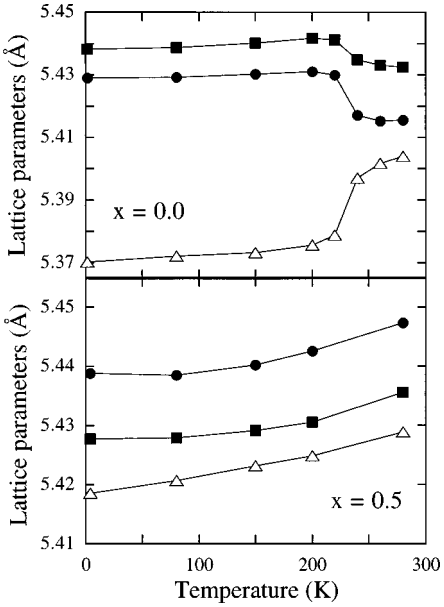

FIG. 6. Temperature dependence of the lattice parameters $\{a(\bullet), b(\blacksquare)$, and $c(\triangle)\}$ for $Pr_{0.6}(Ca_{1-x}Sr_x)_{0.4}MnO_3$ samples with $x=0.0$ and $x=0.5$.

ference in the absolute values of the discontinuities in the Mn-O2 bond lengths produces a decrease in the average bond length which can be associated with the formation of metallic bonding. Discontinuities of this type and magnitude are consistent with the data presented here for samples with $0.25 \leqslant x \leqslant 1.0$ although data points which are closer in temperature around T_C would be required to confirm the presence of this kind of behavior. We note that Caignert *et al.*[31] also observed a decrease in the distortion in a sample of $Pr_{0.7}Ca_{0.25}Sr_{0.05}MnO_3$ at the transition to an AFM ordered

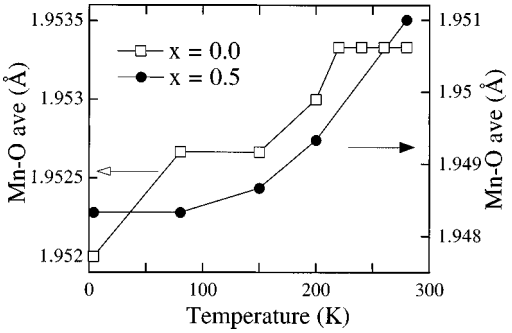

FIG. 8. Variation with temperature of the average Mn-O bond length for samples of $Pr_{0.6}(Ca_{1-x}Sr_x)_{0.4}MnO_3$ with $x=0.0$ and $x=0.5$.

state. In this study we have not observed any anomalies in the structural parameters for samples which order antiferromagnetically which can be directly associated with the magnetic ordering.

Although the structural parameters of these materials show a complex behavior as a function of temperature the variations seen as a function of x are more straightforward. At 280 K, the a lattice parameter increases with x, while the b- and c-axis lattice parameters remain nearly constant across the series (Fig. 10). Thus for small x, $b>a\geqslant c/\sqrt{2}$, while at large x, $a>b>c/\sqrt{2}$ and there is an overall increase in the cell volume with x. At 4 K, for $x=0.00$ $b>a>c/\sqrt{2}$. As the Sr content increases, $a>b>c/\sqrt{2}$ for the *Pbnm* phase. Again there is an overall increase in cell volume with increasing x. At all temperatures the Mn-O-Mn bond angles increase as a function of x (see Fig. 11). In the Ca-rich samples the Mn-O1 is much smaller than Mn-O2 distance. As the Sr content increases the lengths of the two Mn-O2 bonds are split more symmetrically around the Mn-O1. The average Mn-O distance $\langle$Mn-O$\rangle$ decreases with x (Fig. 11).

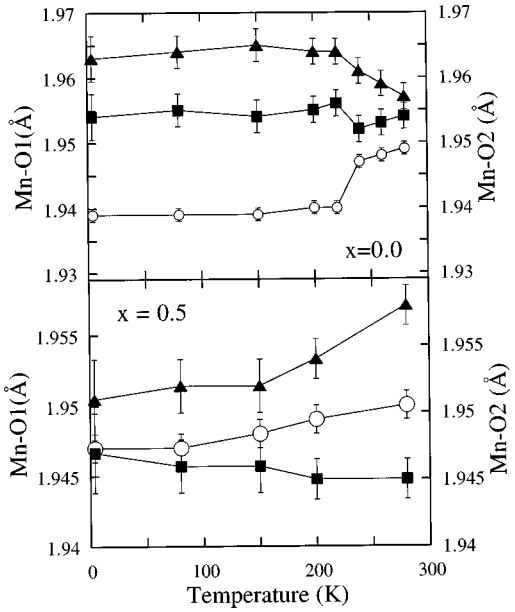

FIG. 7. Temperature dependence of the Mn-O bond lengths {Mn-O1 (○), and Mn-O2 (■ and (▲)} for $Pr_{0.6}(Ca_{1-x}Sr_x)_{0.4}MnO_3$ samples with $x=0.0$ and $x=0.5$.

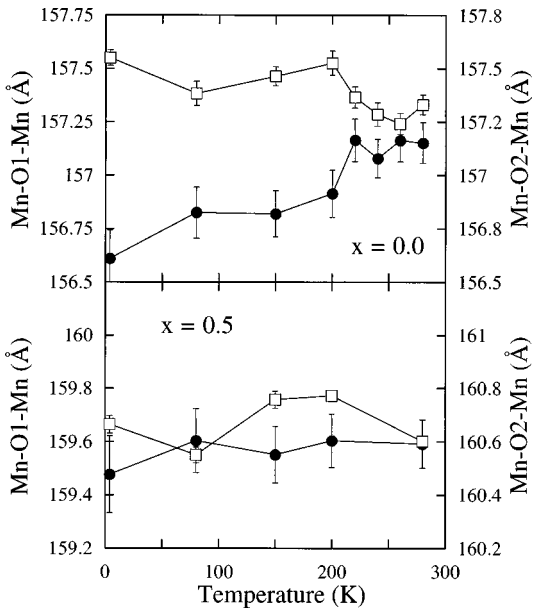

FIG. 9. Temperature dependence of the Mn-O-Mn bond angle {Mn-O1-Mn (●) and Mn-O2-Mn (□)} in samples of $Pr_{0.6}(Ca_{1-x}Sr_x)_{0.4}MnO_3$ with $x=0.0$ and $x=0.5$.

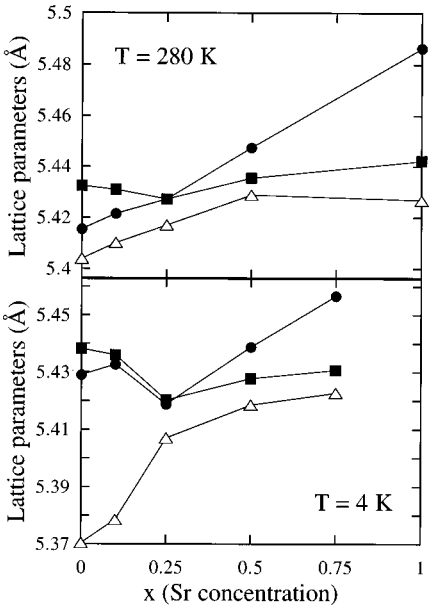

FIG. 10. Lattice parameters {a(●), b(■), and c(△)} versus Sr doping x for samples $Pr_{0.6}(Ca_{1-x}Sr_x)_{0.4}MnO_3$ at 280 and 4 K.

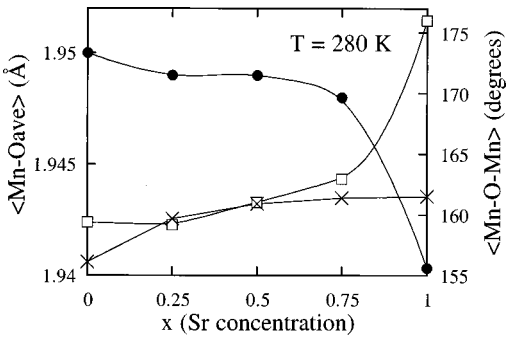

FIG. 11. Variation of the average Mn-O bond length (●) and Mn-O-Mn bond angle {Mn-O1-Mn (□), and Mn-O2-Mn (×)} with the level of Sr doping x in samples $Pr_{0.6}(Ca_{1-x}Sr_x)_{0.4}MnO_3$ at 280 K.

IV. DISCUSSION

The properties of $Pr_{0.6}(Ca_{1-x}Sr_x)_{0.4}MnO_3$ show remarkable sensitivity to changes in x, highlighting the strong correlation between the structural, magnetic, and electronic properties of these manganite materials. There are a number of different models which can be used to help understand this behavior. In the simplest picture we consider the distortions which are introduced into the material by a mismatch in the size of the rare earth and the alkali ions. The tolerance factor $t=(R\text{-O})/\sqrt{2}(A\text{-O})$ (where R-O and A-O are the equilibrium bond lengths) gives a measure of the degree of distortion present. Using the values for ionic radii in 12-fold coordination[32,33] $t\approx 0.96$ for $x=0.0$. This is close to the critical value delineating the boundary between an AFM/insulator and a FM/conductor.[34] t increases with the addition of Sr driving the system toward a FM conducting ground state. The phase diagram shown in Fig. 12 which includes data taken from other work[15] shows that the results of this study are in reasonable accord with this simple model, particularly for samples which are purely FM. At the Ca-rich end the ordering temperature is clearly not a strong function of t.

TABLE III. Selected structural parameters for samples of $Pr_{0.6}(Ca_{1-x}Sr_x)_{0.4}MnO_3$ with $x=0.0$, $x=0.25$, and $x=0.5$. All the refinements were carried out using the higher symmetry orthorhombic *Pbnm* space group. The numbers in parentheses are the statistical errors of the last significant digits.

T (K)	a(Å)	b(Å)	c(Å)	Mn-O1	Mn-O2	Mn-O2	$\langle$Mn-O$\rangle_{ave}$	Mn-O1-Mn	Mn-O2-Mn
$x=0.0$									
280.0	5.4155(1)	5.4325(1)	7.6423(1)	1.949(1)	1.954(2)	1.957(2)	1.9533	157.2(1)	157.33(4)
260.0	5.4152(1)	5.4331(1)	7.6392(1)	1.948(1)	1.953(2)	1.959(2)	1.9533	157.2(1)	157.24(5)
240.0	5.4171(1)	5.4348(1)	7.6324(1)	1.947(1)	1.952(2)	1.961(2)	1.9533	157.1(1)	157.29(6)
220.0	5.4299(2)	5.4412(2)	7.6067(2)	1.940(1)	1.956(2)	1.964(2)	1.9533	157.2(1)	157.37(5)
200.0	5.4310(2)	5.4417(2)	7.6022(3)	1.940(1)	1.955(2)	1.964(2)	1.9530	156.9(1)	157.53(6)
150.0	5.4302(2)	5.4402(2)	7.5989(3)	1.939(1)	1.954(3)	1.965(3)	1.9527	156.8(1)	157.46(4)
80.0	5.4292(2)	5.4387(2)	7.5973(3)	1.939(1)	1.955(3)	1.964(3)	1.9527	156.8(1)	157.38(6)
4.0	5.4290(3)	5.4382(3)	7.5948(3)	1.939(1)	1.954(4)	1.963(4)	1.9520	156.6(1)	157.55(4)
$x=0.25$									
280.0	5.4272(1)	5.4272(1)	7.6607(1)	1.948(1)	1.947(2)	1.955(2)	1.9500	158.9(1)	159.07(2)
200.0	5.4246(1)	5.4246(1)	7.6533(1)	1.946(1)	1.947(2)	1.957(2)	1.95	158.8(1)	158.73(2)
150.0	5.4222(1)	5.4239(1)	7.6495(1)	1.945(1)	1.945(2)	1.955(2)	1.9483	159.0(1)	158.86(3)
80.0	5.4187(1)	5.4205(1)	7.6490(1)	1.945(1)	1.945(2)	1.952(2)	1.9473	158.8(1)	159.05(3)
4.0	5.4188(1)	5.4203(1)	7.6467(1)	1.945(1)	1.944(3)	1.953(3)	1.9473	158.8(2)	159.13(3)
$x=0.50$									
280.0	5.4474(2)	5.4355(2)	7.6776(2)	1.950(1)	1.945(2)	1.958(2)	1.9510	159.6(1)	160.60(2)
200.0	5.4426(1)	5.4306(1)	7.6719(2)	1.949(1)	1.945(2)	1.954(2)	1.9493	159.6(1)	160.77(2)
150.0	5.4402(1)	5.4291(1)	7.6695(2)	1.948(1)	1.946(2)	1.952(2)	1.9487	159.6(1)	160.76(3)
80.0	5.4385(1)	5.4279(1)	7.6659(2)	1.947(1)	1.946(2)	1.952(2)	1.9483	159.6(1)	160.55(3)
4.0	5.4388(1)	5.4277(1)	7.6630(1)	1.947(1)	1.947(3)	1.951(3)	1.9483	159.5(1)	160.67(3)

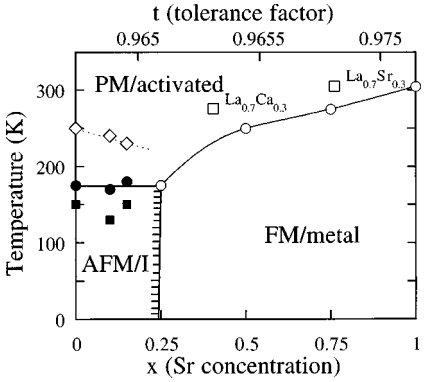

FIG. 12. Phase diagram showing the temperature versus Sr concentration and tolerance factor for samples in the $Pr_{0.6}(Ca_{1-x}Sr_x)_{0.4}MnO_3$ series; (◇) denotes charge-ordering temperature, (●) T_N, (■) T_M, and (○) T_C. Also shown are (□) T_C's for samples of $La_{0.7}Ca_{0.3}MnO_3$ and $La_{0.7}Sr_{0.3}MnO_3$ taken from Ref. 15.

At a more fundamental level, the behavior of these materials has traditionally been explained within the framework of the double-exchange (DE) model[35–37] in which the magnetic coupling between Mn^{3+} and Mn^{4+} ions arises from the motion of electrons between two partially filled Mn d shells with strong on-site Hund's coupling. In $PrMnO_3$ the Mn^{3+} ions have three t_{2g} electrons forming an inert core, while the e_g electron is electronically active with its spin parallel to the core. Doping with divalent Ca and Sr ions means both Mn^{3+} and Mn^{4+} ions are present. The e_g electrons now hop using an intermediate oxygen ion between Mn^{3+} and Mn^{4+} ions via the DE mechanism.[38] Thus DE facilitates electron itinerancy and ferromagnetism. The effective electron transfer $\tilde{t}$ is given by $\tilde{t}=t_{ij}\cos(\theta_{ij}/2)$ where t_{ij} and θ_{ij} denote the electron transfer probability when the localized t_{2g} spins are parallel, and the angle between two neighboring t_{2g} spins, respectively. The mobility of the electrons is expected to increase as $\tilde{t}$ increases. This can be brought about either by aligning the spins using an externally applied magnetic field or alternatively by increasing the bond angle between the manganese and the oxygen ions. In competition with the DE there are several mechanism which increase the localization of the carriers. The JT distortion of the $Mn^{3+}O_6$ state lowers the energy of the e_g electron and impedes hopping to an undistorted e_g state of the Mn^{4+} ion leading the formation of polarons. De Teresa *et al.*[39] have recently reported the presence of magnetic polarons in $La_{0.66}Ca_{0.33}MnO_3$. AFM superexchange produces antiparallel core spin alignment which also inhibits the hopping of the spin polarized e_g electrons. There may be localization effects arising from other sources of non magnetic randomness.[40] There is also the mutual Coulomb repulsion of charge carriers. These effects all produce charge localized or charge ordered systems with AFM order.

This study underlines that there are several competing factors which determine the eventual ground state of the system. In this case doping with Sr does produce an increase in the Mn-O-Mn bond angles with increasing x which should lead to a stronger double-exchange-mediated FM coupling. However, for $x=0.0$ the properties of the system are dominated by the CO and the static JT distortion which occurs at 250 K. The resulting additional localization produces an AFM insulating ground state. The addition of a small amount of Sr does not remove the CO or the JT distortion at 250 K. The magnetic ordering temperature appears to be almost constant. However, below 170 K the magnetic ordering now has both AFM and FM components. A fall in the resistivity of the $x=0.15$ sample at low temperature (see Fig. 2) suggests that the CO is suppressed within the magnetically ordered state although it is not possible to determine if this is the case from the neutron data. It should be noted that the temperature at which the fall in resistivity occurs does not coincide with the onset of FM. Only when the CO and static JT distortions which are observed around 250 K are suppressed does the system order with a simple ferromagnetic structure. Initially T_C is still around 170 K but increases rapidly reaching 305 K at $x=1.0$. Now the fall in resistivity occurs close to T_C.

Finally, it has been suggested that the effects of chemical pressure applied through doping, the application of external pressure, and the application of a magnetic field all play the same role in these materials, namely, to drive the system from a charge ordered antiferromagnetic state which remains insulating down to low temperatures, through a regime where the material first charge orders, then undergoes an insulator metal transition to a conducting state, eventually reaching a regime where the system switches directly from a paramagnetic state with a conductivity which has an activated temperature dependence to a ferromagnetic state with metallic conductivity. Yoshizawa *et al.*[26] have studied the effects of external hydrostatic pressure on the ground-state properties of the $Pr_{0.7}Ca_{0.3}MnO_3$ and confirmed that these three regimes do exist as a function of pressure. Previous work on the properties of $Pr_{1-x}Ca_xMnO_3$ in a magnetic field[19,23] have also identified these three regimes as a function H. The results obtained here and in a previous study on $Pr_{0.65}(Ca_{1-x}Sr_x)_{0.35}MnO_3$ (Ref. 26) clearly demonstrate that these three regimes also exist as a function of doping which acts to apply chemical pressure. It should be noted that external pressure is expected to lead to a decrease in the overall cell volume while doping with Sr increases the cell volume. However, in both cases there is a reduction in the distortion of the Mn-O-Mn bond angle and it is this which dictates the eventual ground state of the system.

[1] S. Jin, T. H. Tiefel, M. McCormack, R. A. Fastnacht, R. Ramesh, and L. H. Chen, Science **264**, 413 (1994).
[2] R. von Helmholt, J. Wecker, B. Holzapfel, L. Shultz, and K. Samwer, Phys. Rev. Lett. **71**, 2331 (1993).
[3] K. Chahara, T. Ohno, M. Kasai, and Y. Kozono, Appl. Phys. Lett. **63**, 1990 (1993).
[4] E. O. Wollan and W. C. Koehler, Phys. Rev. **100**, 545 (1955).
[5] P. Schiffer, A. P. Ramirez, W. Bao, and S.-W. Cheong, Phys. Rev. Lett. **75**, 3336 (1995).
[6] P. G. Radaelli, D. E. Cox, M. Marezio, and S.-W. Cheong, Phys. Rev. B **55**, 3015 (1997).
[7] K. Knizek, Z. Jirak, E. Pollert, F. Zounova, and S. Vratislav, J.

Solid State Chem. **100**, 292 (1992).
[8] Y. Tomioka, A. Asamitsu, Y. Moritomo, H. Kuwahara, and Y. Tokura, Phys. Rev. Lett. **74**, 5108 (1995).
[9] H. Kawano, Y. Tomioka, A. Asamitsu, Y. Moritomo, and Y. Tokura, Science **270**, 961 (1995).
[10] A. Asamitsu, Y. Moritomo, Y. Tomioka, T. Arima, and Y. Tokura, Nature (London) **373**, 407 (1995).
[11] A. J. Campbell, G. Balakrishnan, M. R. Lees, D. McK. Paul, and G. J. McIntyre, Phys. Rev. B **55**, 8622 (1997).
[12] G. H. Jonker and J. H. van Santen, Physica (Amsterdam) **16**, 337 (1950).
[13] G. H. Jonker, Physica (Amsterdam) **22**, 707 (1956).
[14] A. Urushibara, Y. Moritomo, T. Arima, A. Asamitsu, G. Kido, and Y. Tokura, Phys. Rev. B **51**, 14 103 (1995).
[15] H. Y. Hwang, S.-W. Cheong, P. G. Radaelli, M. Marezio, and B. Batlogg, Phys. Rev. Lett. **75**, 914 (1995).
[16] Z. Jirak, S. Vratislav, and J. Zajicek, Phys. Status Solidi **52**, 39 (1979).
[17] E. Pollert, S. Krupicka, and E. Kumzicova, J. Phys. Chem. Solids **43**, 1137 (1982).
[18] Z. Jirak, S. Krupicka, Z. Simsa, M. Dlouha, and S. Vratislav, J. Magn. Magn. Mater. **53**, 153 (1985).
[19] H. Yoshizawa, H. Kawano, Y. Tomioka, and Y. Tokura, Phys. Rev. B **52**, 13 145 (1995).
[20] M. R. Lees, J. Barratt, G. Balakrishnan, D. McK. Paul, and M. Yethiraj, Phys. Rev. B **52**, 14 303 (1995).
[21] Y. Tomioka, A. Asamitsu, Y. Moritomo, and Y. Tokura, J. Phys. Soc. Jpn. **64**, 3626 (1995).
[22] Y. Tomioka, A. Asamitsu, H. Kuwahara, Y. Moritomo, and Y. Tokura, Phys. Rev. B **53**, 1689 (1996).
[23] M. R. Lees, J. Barratt, G. Balakrishnan, D. McK. Paul, and C. D. Dewhurst, J. Phys.: Condens. Matter **8**, 2967 (1996).
[24] J. M. De Teresa, M. R. Ibarra, C. Marquina, P. A. Algarabel, and S. Oseroff, Phys. Rev. B **54**, 12 689 (1996).
[25] J. Rodriguez-Carvajal, Physica B **192**, 55 (1993).
[26] H. Yoshizawa, R. Kajimoto, H. Kawano, Y. Tomioka, and Y. Tokura, Phys. Rev. B **55**, 2729 (1997).
[27] M. Hervieu, G. van Tendeloo, V. Caignaert, A. Maignan, and B. Raveau, Phys. Rev. B **53**, 14 274 (1996).
[28] C. Ritter, P. G. Radaelli, M. R. Lees, J. Barratt, G. Balakrishnan, and D. McK. Paul, J. Solid State Chem. **127**, 276 (1996).
[29] P. G. Radaelli, M. Marezio, H. Y. Hwang, S.-W. Cheong, and B. Batlogg, Phys. Rev. B **54**, 8992 (1996).
[30] D. N. Argyriou, J. F. Mitchell, C. D. Potter, D. G. Hinks, J. D. Jorgensen, and S. D. Bader, Phys. Rev. Lett. **76**, 3826 (1996).
[31] V. Caignaert, E. Suard, A. Maignan, Ch. Simon, and B. Raveau, J. Magn. Magn. Mater. **153**, L260 (1996).
[32] R. D. Shannon, Acta Crystallogr., Sect. A: Cryst. Phys., Diffr., Theor. Gen. Crystallogr. **32**, 751 (1976).
[33] Y. Q. Jia, J. Solid State Chem. **94**, 184 (1991).
[34] W. Archibald, J.-S. Zhou, and J. B. Goodenough, Phys. Rev. B **53**, 14 445 (1996).
[35] C. Zener, Phys. Rev. **82**, 403 (1951).
[36] P. W. Anderson and H. Hasegawa, Phys. Rev. **100**, 675 (1955).
[37] P-G. de Gennes, Phys. Rev. **118**, 141 (1960).
[38] Millis *et al.* have shown that the DE alone is not sufficient to explain the magnitude of magnetoresistance observed in the manganite materials and that additional physics involving a strong *J-T* distortion may be required. A. J. Millis, P. B. Littlewood, and B. I. Shraiman, Phys. Rev. Lett. **74**, 5144 (1995); **77**, 175 (1996).
[39] J. M. de Teresa, M. R. Ibarra, P. A. Algarabel, C. Ritter, C. Marquina, J. Blasco, J. Garcia, A. del Moral, and Z. Arnold, Nature (London) **386**, 256 (1997).
[40] L. Sheng, D. Y. Xing, D. N. Sheng, and C. S. Ting, Phys. Rev. Lett. **79**, 1710 (1997).